Journal of the Brazilian Society of Mechanical Sciences and Engineering (2018) 40:184
https://doi.org/10.1007/s40430-018-1108-6

TECHNICAL PAPER

Effect of nanoclay and bolt preloads on the strength of bolted joints in glass epoxy nanocomposites

Kulwinder Singh Chani[1] · J. S. Saini[1] · H. Bhunia[2]

Received: 13 October 2017 / Accepted: 28 February 2018 / Published online: 17 March 2018

Abstract
The present work deals with the effect of different molding parameters and bolt pretension on the performance of single-lap joints. Bolt joints were prepared from woven glass fiber reinforced laminates incorporating nanoclay content which was varied from 0 to 5 wt%. Curing parameters for the nanocomposite manufacturing were optimized using the Taguchi method. Different geometric parameters, i.e., edge distance-to-hole diameter (*E*/*D*) ratio and width-to-hole diameter (*W*/*D*) ratio, were varied over the range of 2–5. To analyze the effect of bolt preloads, different levels of preloads, i.e., 0, 3, and 5 Nm, were considered for the failure analysis of the joint. Progressive damage analysis along with the characteristic curve method and Hashin failure criteria was performed to predict the failure load and failure modes in the bolted joints, numerically. Failure load was improved by 19 and 37% for joints with 3 and 5 Nm torque, respectively.

Keywords Woven glass fiber · Nanoclay · Taguchi method · Bolt joints · Preloads · Characteristic curve

1 Introduction

Development of lightweight and high-performance materials is the need of today's engineering world. To increase power-to-weight ratio, aircraft, automotive, marines, and defense industries are focusing on alternative materials to the traditional metals. Therefore, composite materials having a high strength-to-weight ratio are being preferred and are under huge research and development. Fiber reinforced plastics (FRP) being part of the composite materials family are getting attention for manufacturing different components for various applications. The number of applications requires the components to be joined together. Mechanical and adhesive joints are mainly used for joining of different parts prepared from composite materials. Mechanical joints are preferred over adhesive joints as they facilitate disassembly when required. Various studies have been performed by different researchers to analyze the effect of different parameters, such as the type of fastener, bolt-hole clearance, preloads, geometric ratios, material and fiber orientation etc., on the performance of the mechanical joints.

Sen et al. [1] carried out experimental investigations on bearing strength and failure modes of the bolted joints prepared from the glass fiber reinforced polymer composite laminates. Geometrical parameters, i.e., *E*/*D* and *W*/*D*, were varied from 1–5 and 2–5, respectively. In addition, different fiber orientations to assess the material contribution and different level of preloads were applied. McCarthy et al. [2] analyzed the bolt-hole clearance effects by performing a 3D numerical analysis on single-bolt single-lap composite joints. Zhai et al. [3] performed experimental investigations to analyze the effects of bolt torque and bolt-hole clearance on the bearing response of single-bolt joints. Qin et al. [4] carried out the experimental and numerical studies to analyze the effects of different types of bolt heads, i.e., protruding and countersink head on the mechanical behavior of the double-lap composite joint. Zhang et al. [5] carried out numerical studies on the failure of multi-bolt joints using a progressive damage analysis based characteristic length method. Atas and Soutis [6] used cohesive zone elements (CZEs) to develop a strength prediction method for composite bolted joints. Egan et al.

Technical Editor: Pedro Manuel Calas Lopes Pacheco.

✉ Kulwinder Singh Chani
kulwinder.singh@thapar.edu

[1] Mechanical Engineering Department, Thapar University, Patiala, Punjab 147004, India

[2] Chemical Engineering Department, Thapar University, Patiala, Punjab 147004, India

[7] modeled bolt-hole clearance to address the manufacturing limitations for the single-lap joints with countersunk fasteners using the Abaqus software. Gray et al. [8] investigated the effects of laminate thickness, missing fasteners, and laminate taper on the strength and stiffness of single-lap joints. On the other hand, to increase the performance of the composite materials, fillers are being used by different researchers. Nanofillers mixed in epoxy increase the mechanical properties of the material. Arun et al. [9] compared the performance of unfilled composite bolted joints with TiO_2 and ZnS filled composite joints under tensile loading. Sekhon et al. [10] investigated the effect of nanoTiO_2 and nanoclay on the bearing strength of the single pin joint made of glass epoxy composite laminates. Asi [11] investigated the effects of Al_2O_3 microfillers on the bearing strength of pinned joints.

Concluding the literature review, it is observed that geometric parameters, i.e., *E*/*D* and *W*/*D* ratios, and stacking sequence affect the performance of mechanical joint significantly. Preloads have increased the ultimate failure load and the initial joint stiffness for the bolted joints. On the other hand, fillers have shown improvements in the mechanical properties of the composite material by improving matrix properties individually and at the interface of the fiber and the matrix. Therefore, the present study is focused on the effect of nanofiller, i.e., nanoclay on the mechanical performance of single-lap single-bolt joint. Effect of different geometric parameters and bolt preloads has been studied both experimentally and numerically in the material with and without the nanoclay content.

2 Experimentation

The following section describes the materials, manufacturing method, and testing procedures followed in the present work.

2.1 Materials

2.1.1 Glass fiber

Advantex E-glass 2D woven fabric with 360 gsm and plain weave construction used as reinforcement was supplied by Owens Corning India Pvt. Ltd., Mumbai, India. The mechanical and physical properties of the glass fiber used in the present work are shown in Table 1.

2.1.2 Resin

The DGEBA-based epoxy (L-12), hardener (K-12), and accelerator (K-13), supplied by Atul Ltd., Gujarat, India, were used in the present work. The modulus of elasticity, tensile strength, flexural strength, and compressive strength of the supplied resin were 15–16 GPa, 70–90 MPa, 100–120 MPa, and 190–210 MPa, respectively.

2.1.3 Nanoclay

Natural Montmorillonite Modified Cloisite® 30B was used as nanofillers to enhance the mechanical properties of the epoxy. Typical properties of the nanoclay are shown in Table 2.

2.1.4 Fastener

High tensile fasteners manufactured by commercial available brand "Unbrako" with a metric size of 4 mm in diameter have been used in the present work. Lock nut has been used to avoid undesired loosening of the nut–bolt assembly. The mechanical properties of the fasteners used in single-lap joints are shown in Table 3.

2.2 Composite preparation

The process starts with the cutting of the 2D woven glass fabric from the roll to adequate size for the compression molding. After cutting a sufficient number of laminas, epoxy resin is prepared as per ratio provided by the supplier shown in Table 4. To analyze the effect of nanoclay on the performance of glass epoxy composite, two different types of materials have been prepared. One is fiber reinforced in neat epoxy and other is fiber reinforced in epoxy modified with nanoclay.

The laminate of desired thickness is prepared using the hand-layup technique. Once the composite laminate is ready, it is cured at room temperature for 36–48 h. The laminate is then cured in compression molding machine. The curing parameters used in compression molding machine are optimized for maximizing the mechanical properties of the laminates prepared from the selected material.

2.2.1 Optimization of curing parameters

The temperature and pressure affect the laminate thickness and void content, which in turn have significant effects on the mechanical properties of the composite laminates [12]. Moreover, catalyst mixed in epoxy resin starts reaction at room temperature; and according to the current process, before putting into the compression mold, laminates are kept at room temperature for 36–48 h depending upon the environmental conditions. The prephase time, i.e., time to build up curing temperature in compression mold is more than 30 min in general and the laminates are kept in the mold during this temperature ramp-up time. Therefore, it

Table 1 Physical and mechanical properties of the glass fabric

Property	Test method	Value
Density	ASTM D1505	2.62 g/cc
Thermal linear expansion 0–300 °C	ASTM D696	6 ppm/C
Softening point	ASTM C338	916 °C
Tensile strength at 23 °C	ASTM D2101	3100–3800 MPa
Elastic modulus	Sonic Method	80–81 GPa
Elongation at the breaking load	ASTM D2101	4.6%

Table 2 Typical properties of the nanoclay

Organic modifier	Modifier concentration	Typical dry particle size	Purity	Moisture	Weight loss on ignition
MT2EtOH	90 meq/100 g clay	< 80 nm	99%	< 2%	30%

Table 3 Mechanical properties of the fastener

Description	Material	Ultimate tensile strength (MPa)	Tensile load (kN)
4 mm dia socket head cap screw	Alloy steel	1300	11.4

Table 4 Processing properties of the epoxy resin

Property	Resin: hardener: accelerator mix ratio (by wt.)	Initial mix viscosity	Pot life of mix (< 5 kg)	Gel time
Condition	–	@ 40 °C	@ 80 °C	@ 80 °C
Unit	w/w	cPs	Min	Min
Value	100:100:0.1–2	450	60	150

was important to optimize process parameters, i.e., pressure, temperature, and hold time for curing composite laminates in compression molding machine. To reduce the number and cost of experimentation, the design of experiments is used in the present work. For the design of experiment, many techniques are available out of which Taguchi method is commonly used to reduce the number of experimental trials.

2.2.2 Taguchi method

Taguchi developed a family of fractional factorial experimental matrices, called orthogonal arrays (OAs), which can be used under various situations to optimize the process parameters and improve the results [13–16]. To calculate the deviation between desired and experimental values of performance characteristic, a loss function is defined, which is further transformed into signal-to-noise (*S*/*N*) ratio. *S*/*N* ratio is further classified as follows:

$$\text{Nominal is the best}: \frac{S}{N} = 10\log\left(\frac{\bar{y}}{S_y^2}\right), \tag{1}$$

$$\text{Larger is the better}: \frac{S}{N} = -10\log\left(\frac{1}{n}\sum_{i=1}^{n}\frac{1}{y_i^2}\right), \tag{2}$$

$$\text{Smaller is the better}: \frac{S}{N} = -10\log\left(\frac{1}{n}\sum_{i=1}^{n}y_i^2\right), \tag{3}$$

where $\bar{y}$ is the average of observed data, n is the number of observations, S_y^2 the variance of y, and y is the observed data.

In the present study, the objective is to maximize the strength of the material. Therefore, Eq. (2), i.e., 'Larger is the better', is used to calculate the *S*/*N* ratios.

In the present study, three factors, i.e., pressure, temperature, and holding time, with four levels each have been selected for analysis. The degree of freedom of the problem is 9. A fractional factorial design using standard L_{16} orthogonal array having 15 degree of freedom, which is larger than the degree of freedom of the current problem, has been adopted here. Different levels of control factors

Table 5 Factors and levels considered in compression molding process

Factor	Levels			
	0	1	2	3
A—pressure (kN)	100	120	140	160
B—temperature (°C)	90	120	150	180
C—hold time (min)	10	20	30	40

are shown in Table 5. The numerical values of these factors are carefully selected by the authors based on the literature review and lot of the initial experimentations done by the authors on the raw material. The selected values of the parameters narrowed down the variation in the tensile and compression strength of the laminates.

The tensile and compressive testing of the laminates is done as per procedure defined in ASTM D3039 and D695, respectively. Figure 1 shows the specimen configuration for tensile and compressive testing of the laminates. For the compression testing, due to less thickness of the specimen, i.e., 2.5 mm, a support jig was used as recommended in the ASTM D695.

The tensile and compressive strengths for the different experimental runs are shown in Table 6. These tests were conducted on German make Zwick–Roell Universal Testing Machine.

To determine the best values of temperature, pressure, and hold duration that simultaneously maximizes the tensile and compressive strength, the values of both tensile and compressive strength are normalized in the range of 0–1 to get a comparable sequence. μ_t and μ_c are the membership functions [14] associated with tensile and compressive strength, respectively, and are defined by Eqs. (4) and (5):

$$\mu_t = 1 - \frac{T}{T_{max}}, \tag{4}$$

$$\mu_c = 1 - \frac{C}{C_{max}}, \tag{5}$$

where T and C are the normalized values of tensile and compressive strength, respectively, which are calculated using Eq. (6) corresponding to each experimental trial. Based on experimental results, T_{max} and C_{max} are the maximum normalized values of tensile and compressive strength. For the simultaneous maximization of tensile and compressive strength, the area A (FGHIJF) shown in Fig. 2 should be as maximum as possible. The area A can be calculated using Eq. (7):

$$X_n = \frac{X_i - \min}{\max - \min}, \tag{6}$$

$$A = \frac{1}{2}[T(1-\mu_t) + C(1-\mu_c)]. \tag{7}$$

Normalized values (0–1) of the tensile and compressive strength of the composite laminates prepared in different experimental runs are listed in Table 7. Taking area (A) as a single response, *S*/*N* ratios have been calculated. The reaction rate of epoxy increases and curing time decreases with increase in cure temperature [17, 18]. Using the calculated *S*/*N* ratio, analysis of means has been performed and is shown in Table 8. The table also shows the rank of the process parameters affecting the multi-performance response based on the Delta (Δ) statistics.

From the *S*/*N* ratio graph shown in Fig. 3, it is clearly visible that the curing temperature has a significant effect on the mechanical strength of the composite material. As the mold set temperature increases, the degree of cure of the epoxy increases resulting in higher mechanical properties. As shown in *S*/*N* ratio plots, the effect of curing time is significantly reduced beyond 30 min. As seen in the *S*/*N* ratio plots, increasing pressure from 100 to 140 kN increases the strength of the composite material. The cure pressure has shown significant improvements in the mechanical properties of the composite materials as it reduces the void content [12]. Hence, the optimum strength can be achieved using the pressure of 140 kN, temperature of 150 °C, and holding time of 30 min.

The relative significance of the process parameters is established using analysis of variance (ANOVA), as shown in Table 9. The P value below 0.05 (at 95% confidence interval) for all parameters shows that all the process parameters are significant. The results obtained are verified by performing confirmation test at optimized process parameters. The confirmation test for tensile and compressive strengths gave the values as 410 and 270 MPa, respectively, which are greater in comparison to all responses shown in Table 6.

2.2.3 Preparation of nanocomposite

To add the nanoclay in the epoxy, desired wt% of nanoclay is mixed in the hardener with a high viscous stirrer at 8000 rpm. The viscosity of the hardener is lesser than the epoxy resin, which eventually helped to mix the nanoclay into the epoxy. The mixture is then placed in probe sonicator for 70 min. To increase the efficiency of the probe sonicator, small quantities of the mixture are used in repeated cycles. After completion of the sonication process, the epoxy resin is again mixed using high viscous stirrer for 10 min at 8000 rpm. The resultant mixture is then used for the preparation of the laminates using hand-layup technique.

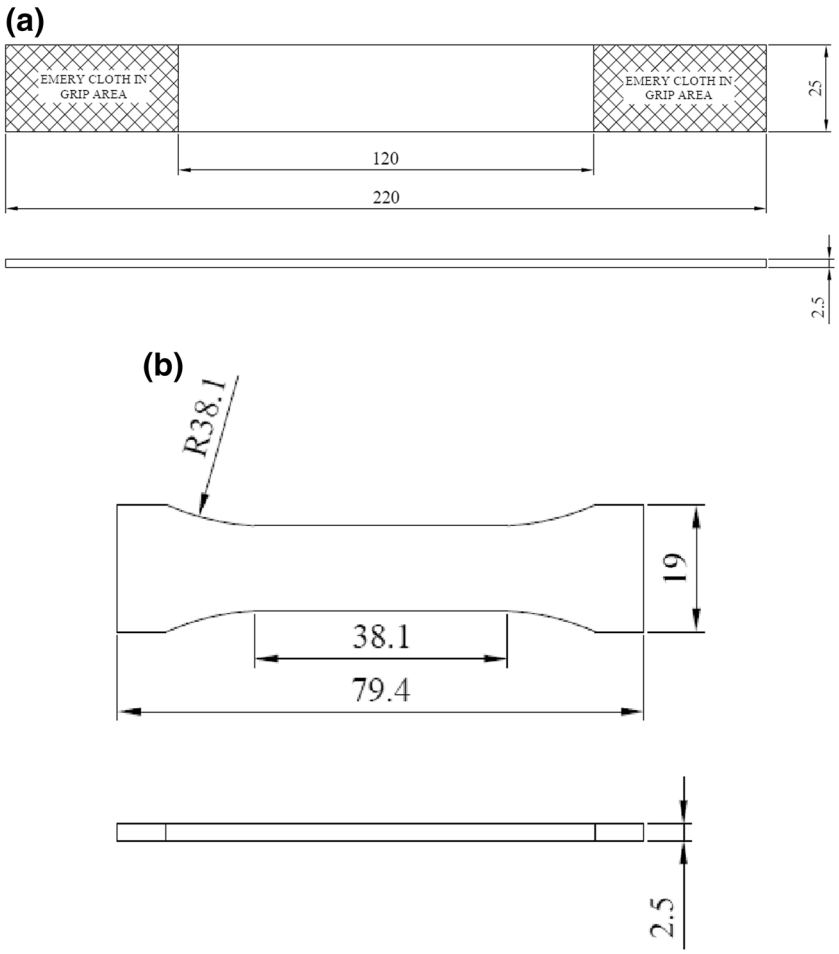

Fig. 1 Specimen configuration for the **a** tensile test, and **b** compression test

Table 6 Tensile and compressive strength of the laminates cured at different levels of pressure, temperature, and duration

Experimental run	Factor			Tensile strength (MPa)	Compressive strength (MPa)
	A	*B*	*C*		
1	0	0	0	349	199
2	0	1	1	368	212
3	0	2	2	377	234
4	0	3	3	378	227
5	1	0	1	368	190
6	1	1	0	377	216
7	1	2	3	390	249
8	1	3	2	390	246
9	2	0	2	377	234
10	2	1	3	390	249
11	2	2	0	390	243
12	2	3	1	395	256
13	3	0	3	377	230
14	3	1	2	390	244
15	3	2	1	395	250
16	3	3	0	390	238

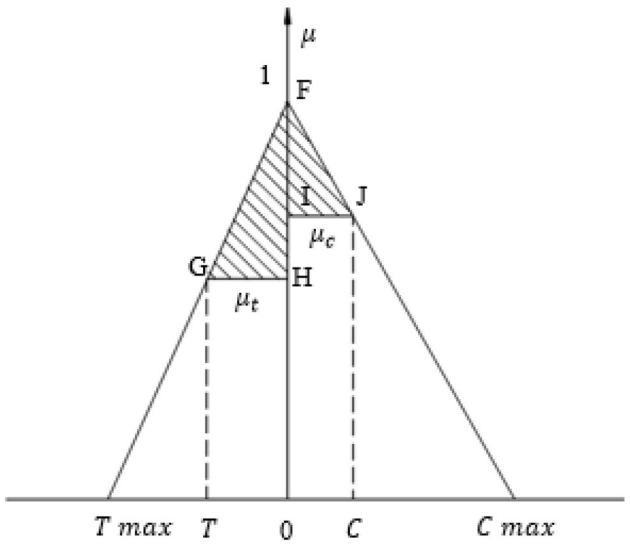

Fig. 2 Membership functions for tensile and compressive strength of the composite laminates

2.2.4 Estimation of appropriate wt% of nanoclay

Nanoclay particles have proved to trigger a tremendous improvement in the properties of the polymers in which they are dispersed [19–22]. Such enhancement in the properties of nanocomposites occurs mostly due to their unique phase morphology and improved interfacial properties [23].

To determine the appropriate wt% of nanoclay required to be mixed in the epoxy, nanoclay concentration is varied from 0 to 5 wt%. Tensile strength for each nanocomposite after varying the nanoclay contents from 0 to 5 wt% is shown in Fig. 4. It is observed that the tensile strength of the nanocomposite material increases with increasing the amount of nanoclay content up to 3 wt%. As can be seen from Fig. 4, there is about 20% increase in the strength with 3 wt% of nanoclay content as compared to plain glass fiber epoxy.

The increase in tensile strength up to 3 wt% of nanoclay was due to increase in the specific surface area of the nanocomposite material. However, increasing nanoclay concentration beyond 3 wt% resulted in the formation of the agglomerates which eventually decreased the specific

Table 7 Experimental run, normalized values, area, and signal-to-noise ratio

Experiment no.	Normalized value		Area	Signal-to-noise ratio
	Tensile strength	Compressive strength		
1	0	0.136364	0.009298	− 40.6327
2	0.413043	0.333333	0.140858	− 17.0244
3	0.608696	0.666667	0.407477	− 7.7979
4	0.630435	0.560606	0.355864	− 8.9743
5	0.413043	0	0.085302	− 21.3808
6	0.608696	0.393939	0.262849	− 11.6059
7	0.891304	0.893939	0.796776	− 1.9733
8	0.891304	0.848485	0.757175	− 2.4161
9	0.608696	0.666667	0.407477	− 7.7979
10	0.891304	0.893939	0.796776	− 1.9733
11	0.891304	0.80303	0.719641	− 2.8577
12	1	1	1	0.0000
13	0.608696	0.606061	0.36891	− 8.6616
14	0.891304	0.818182	0.731922	− 2.7107
15	1	0.909091	0.913223	− 0.7885
16	0.891304	0.727273	0.661675	− 3.5871

Table 8 Response for signal-to-noise ratios

Process parameters	Level 1	Level 2	Level 3	Level 4	Δ (max–min)	Rank
A (pressure)	− 18.607	− 9.344	− 3.157	− 3.937	15.450	2
B (temperature)	− 19.618	− 8.329	− 3.354	− 3.744	16.264	1
C (duration)	− 14.671	− 9.798	− 5.181	− 5.396	9.490	3

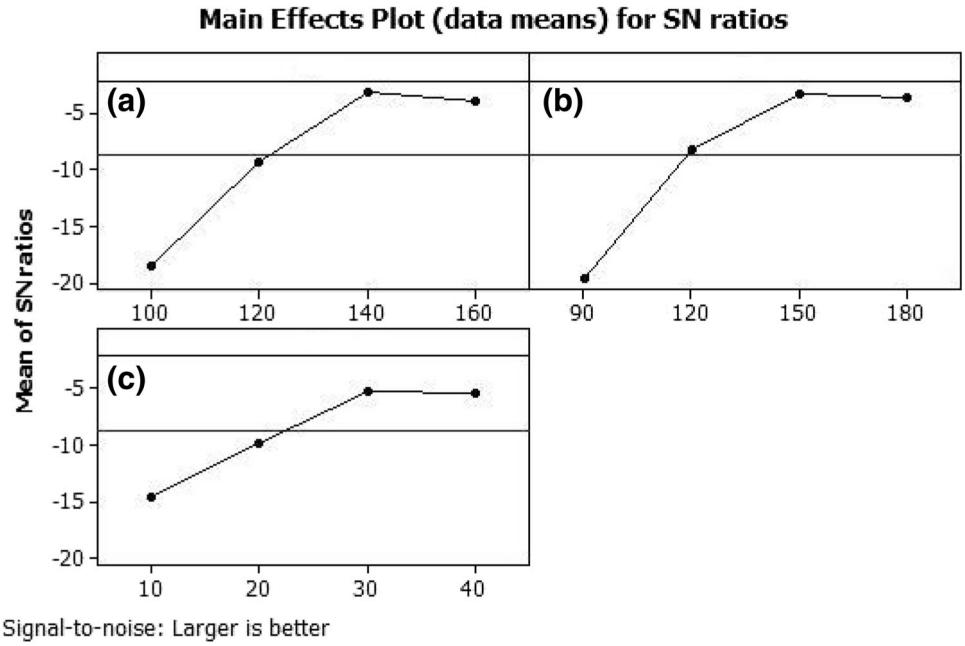

Fig. 3 *S/N* ratio plots of the combined response of the tensile and the compressive strength of the laminates cured at different levels of **a** pressure, **b** temperature, and **c** duration

Table 9 Analysis of variance for *S/N* ratios

Source	*df*	Seq SS	Adj SS	Adj MS	*F*	*P*
A (pressure)	3	607.85	607.85	202.62	14.14	0.004
B (temperature)	3	689.86	689.86	229.95	16.04	0.003
C (duration)	3	240.59	240.59	80.20	5.60	0.036
Residual error	6	85.99	85.99	14.33		
Total	15	1624.29				

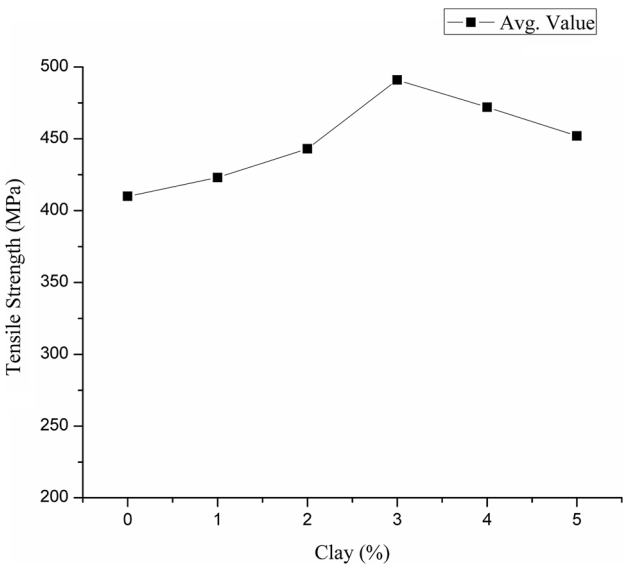

Fig. 4 Effect of nanoclay wt% on the tensile strength of the composite laminate

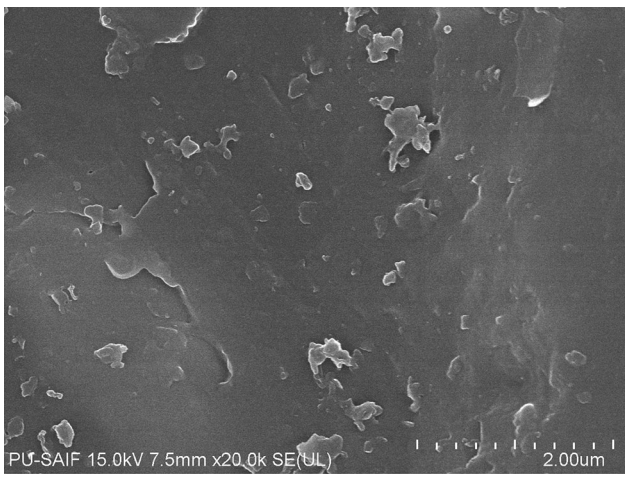

Fig. 5 FESEM micrograph of epoxy modified with 3 wt% of nanoclay

surface area and resulted in the reduced tensile strength of the nanocomposite.

FESEM micrograph of epoxy with 3 wt% of nanoclay content is shown in Fig. 5. The figure shows the uniform distribution of nanoclay in epoxy.

2.2.5 Material characterization

The laminates were prepared at the optimized values of the curing parameters, i.e., pressure, temperature, and duration. Tensile, shear, and compression testing has been done as per the procedure defined in ASTM D3039, D5379 and D695, respectively. The specimen configurations for tensile and compression testing are shown in Fig. 1. The specimen

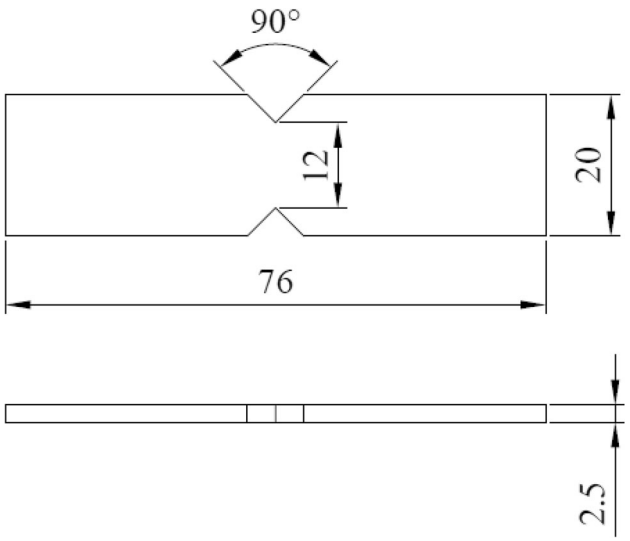

Fig. 6 Specimen configuration for the shear test

configuration for shear testing is shown in Fig. 6. The mechanical properties of the prepared composite laminates are shown in Table 10.

2.3 Lap joint

Lap joint was prepared from the laminates which were characterized at optimum values of pressure, temperature, and curing time for maximum strength. To fabricate the single-lap joint, composite laminates were cut to the desired size using diamond cutter followed by drilling a hole of 4 mm diameter. While drilling, a flat plywood is firmly held below the specimen to avoid delamination at the outer layer when drill passes through the other side of the specimen. Thereafter, the two strips of the cut specimen were assembled using nut, bolt, and washer to form a lap joint. The geometry of the lap joint is shown in Fig. 7.

To analyze the joint for different geometric parameters, the values of *E*/*D* and *W*/*D* ratios were varied from 2–5. The different design configurations of bolt joint by varying different geometric parameters are shown in Table 11.

2.4 Results and discussion

Tensile tests were performed on the single-lap joint on Zwick–Roell Universal Testing Machine, as shown in Fig. 8, at a crosshead speed of 2 mm/min. Minimum three specimens were tested for each configuration. The average failure loads for each experimental set are shown in Table 12. It can be seen from the table that the failure load increases with increase in *E*/*D* and *W*/*D* ratios.

The failure behaviors of single-lap joints prepared from the laminates made without and with nanoclay content are shown in Figs. 9 and 10, respectively. It is observed that the load–displacement curves were linear up to the initial failure, i.e., the first peak point of the curve. To predict the ultimate failure of the joint, the load was further increased. With the increase in the load, there was more increase in the strain rate as compared to the stress rate which was due to the fact that the material already had an initial failure. Moreover, with the increase in load, there came the effect of eccentric loading and then the secondary bending which may also contributed into the non-linear nature of the curve.

As shown in Figs. 9a and 10a, increasing *E*/*D* ratio for the joints with $W/D = 2$, not much improvement in failure load is observed. There is sudden drop in the load displacement curve which represents the net-tension type of failure mode. This is because of the less margin between the hole and the side edge of the specimens. The failure load increases with increase in both *E*/*D* and *W*/*D* ratios. For $W/D = 4$ and 5, as shown in Figs. 9c, d, 10c, d, increasing *E*/*D* ratio has shown a significant improvement in the failure load. Comparing joint configurations with identical *E*/*D* ratios, it is clear from Figs. 9 and 10 that increasing *W*/*D* ratio has increased the maximum displacement to the ultimate failure of the joint. For $W/D = 4$ and 5, maximum displacement to the ultimate failure is quite large. The load displacement curve moves forward in a zig-zag pattern with the multiple peak points which represents the bearing failure mode.

Table 10 Mechanical properties of the composite laminates prepared at optimized molding parameters

Property	Symbol (units)	Without nanoclay	With nanoclay of 3 wt%
Longitudinal modulus in tension	E_1 (GPa)	21.68	27.04
Transverse modulus in tension	E_2 (GPa)	21.68	27.04
Longitudinal strength in tension	X_t (MPa)	410	491
Transverse strength in tension	Y_t (MPa)	410	491
Longitudinal strength in compression	X_c (MPa)	270	327
Transverse strength in compression	Y_c (MPa)	270	327
Shear strength	S (MPa)	104	114.4
Poisson ratio	ν_{12}	0.148	0.139

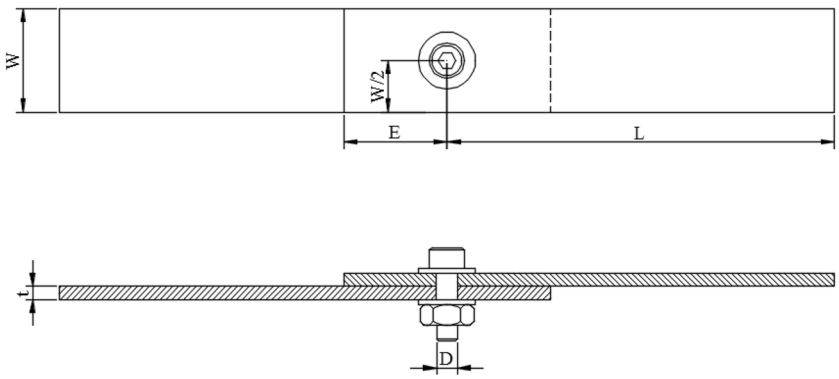

Fig. 7 Geometry of single-lap joint

Table 11 Geometry of the specimens tested under tensile load

Ratios	Diameter of hole (mm)	*E* (mm)	*W* (mm)	Thickness (mm)	Length from hole to edge (mm)
W/D = 2					
E/D = 2	4	8	8	2.5	80
E/D = 3	4	12	8	2.5	80
E/D = 4	4	16	8	2.5	80
E/D = 5	4	20	8	2.5	80
W/D = 3					
E/D = 2	4	8	12	2.5	80
E/D = 3	4	12	12	2.5	80
E/D = 4	4	16	12	2.5	80
E/D = 5	4	20	12	2.5	80
W/D = 4					
E/D = 2	4	8	16	2.5	80
E/D = 3	4	12	16	2.5	80
E/D = 4	4	16	16	2.5	80
E/D = 5	4	20	16	2.5	80
W/D = 5					
E/D = 2	4	8	20	2.5	80
E/D = 3	4	12	20	2.5	80
E/D = 4	4	16	20	2.5	80
E/D = 5	4	20	20	2.5	80

Incorporating 3 wt% of nanoclay compared to the joints prepared with neat epoxy has increased the failure load in almost all joint configurations. There is a significant improvement of about 15–20% with the addition of nanoclay for configurations $W/D > 3$ and $E/D > 3$. This is due to the promoted interfacial bonding between fiber and epoxy. Mechanical properties of the epoxy are also improved as an individual using nanofillers.

The failure modes for different joint configurations with and without nanoclay are shown in Table 13. A pure bearing failure mode is observed in all $W/D = 5$ joint configurations for joints prepared from laminates without nanoclay. However, in case of joints prepared from laminates with nanoclay, pure bearing is seen in $W/D \geq 4$ and $E/D \geq 4$ joint configurations. Figure 11 shows actual images of some of the specimens depicting the failure modes. Comparing specimen prepared with and without the nanoclay for $W/D = 4$ and $E/D = 3$ joint configuration, as shown in Fig. 11a, b, it is clearly seen that nanoclay has improved the failure mode from bearing + net-tension to the pure bearing. It is also seen that the maximum displacement before catastrophic failure is increased by increasing edge and width of the specimen. Larger values of edge and width facilitates more time before the complete loss of the joint strength and functionality. Hence, keeping $W/D \geq 4$ and $E/D \geq 4$ will lead to a bearing mode

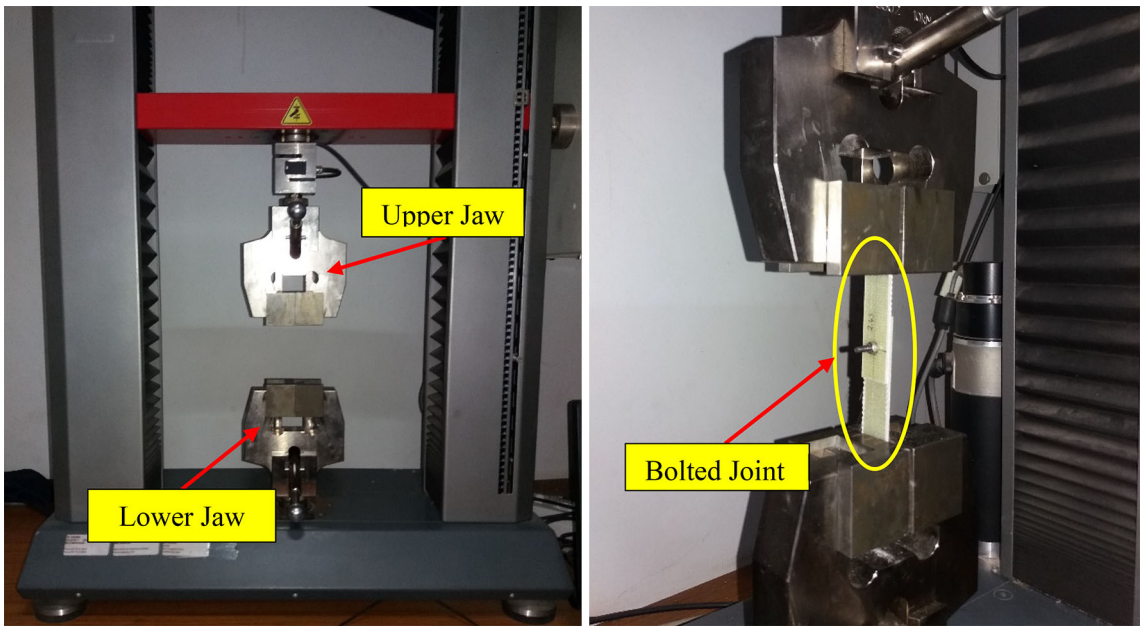

Fig. 8 Tensile testing of the single-lap joint on universal testing machine (UTM)

Table 12 Failure loads obtained in different experimental sets

Set no.	Ratios		Failure load (N)	
	W/D	*E/D*	Neat	Clay
1	2	2	2327	2357
2	2	3	2427	2480
3	2	4	2500	2545
4	2	5	2654	2694
5	3	2	2990	3315
6	3	3	3609	4147
7	3	4	4000	4852
8	3	5	4205	4884
9	4	2	3618	3878
10	4	3	4405	4868
11	4	4	4800	5309
12	4	5	5290	5668
13	5	2	3981	4457
14	5	3	4905	5263
15	5	4	5345	5963
16	5	5	5610	6294

of failure and reduce the chance of sudden uninformed failures.

A comparison of maximum failure loads for all joint configurations prepared from laminates with neat epoxy and with 3 wt% of nanoclay is shown in Fig. 12. It is clearly seen from the figure that incorporating the nanoclay into the epoxy has improved the maximum failure load by about 18%.

2.4.1 Effect of preloads in the bolted joint

In case of mechanically fastened joints, bolt tightening torque is an important factor which is necessary for locking of the joint in place and significantly affects the performance of the joint. To analyze the effect of preloads on the joint performance, the geometry configuration of *E/D* and *W/D* was fixed to 4 as the joint with *E/D* and *W/D* $\geq$ 4 had the bearing failure mode. The torque on the said configuration was varied from 0 to 5 Nm. Hand tightening is assumed to be having a torque of 0 Nm. The effect of increasing the torque on the strength of the joint is shown in Fig. 13. Failure load increases with increasing bolt preloads. It is clear from Fig. 13 that increasing torque reduces the maximum displacement before the ultimate failure. The specimens with higher torque values have less displacement to failure compared to the specimens with lower torque settings. Comparing neat and clay joint configurations, increased joint stiffness is observed for the joints prepared from laminates with nanoclay content.

Comparison of maximum failure load for the composite joints prepared from neat and nanoclay considering torque variation has been presented in Fig. 14. It is observed that increasing bolt preloads significantly improves the failure load and hence the joint performance. For joints prepared from laminates without nanoclay, failure load increased by 19 and 37% with increasing torque from 0 to 3 and 5 Nm, respectively. Comparing neat and nanoclay joint configurations, almost the same amount of improvement is imparted to joint performance increasing preloads to the equal levels.

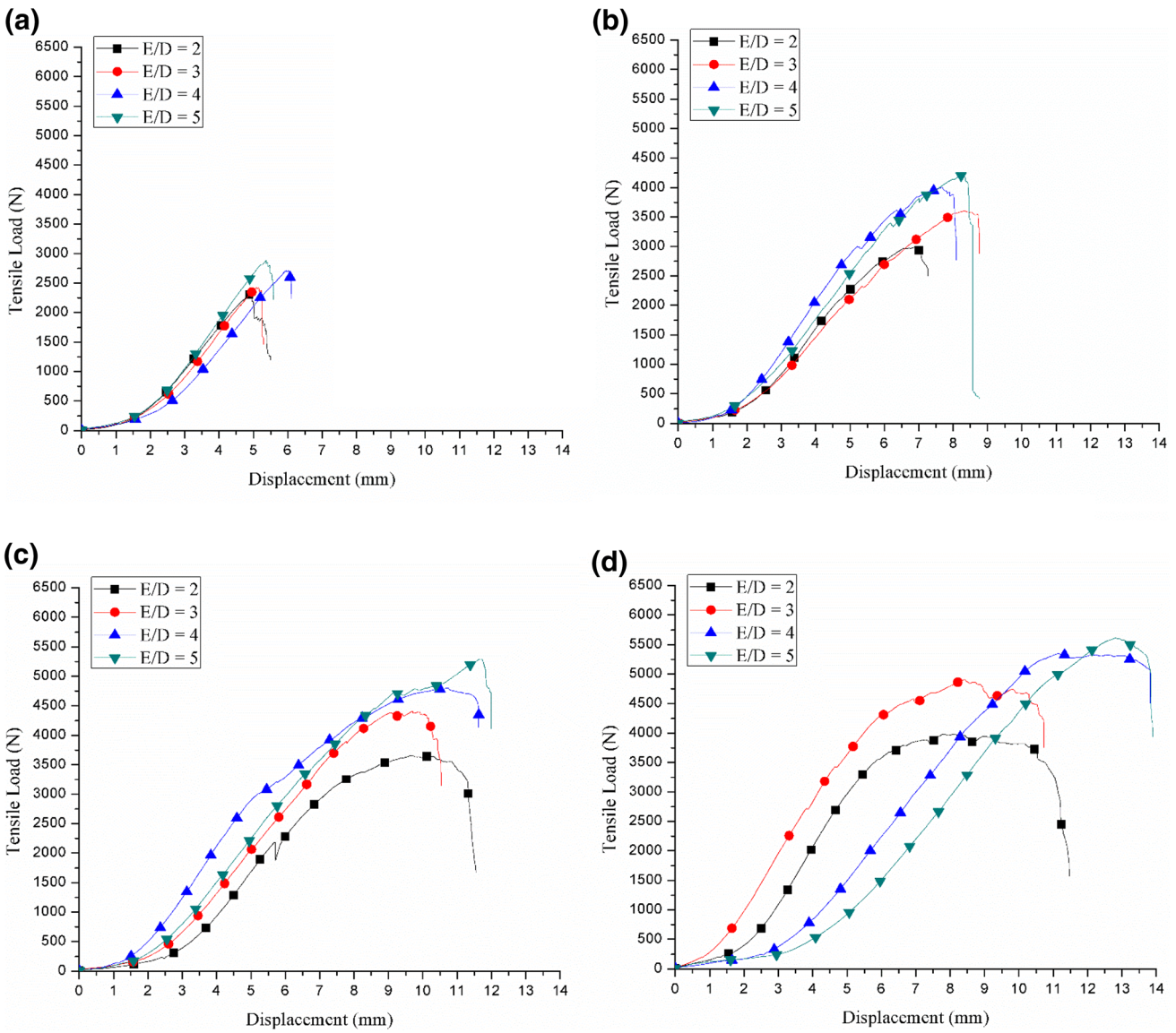

Fig. 9 Load vs displacement plots for the joints without nanoclay with 0 Nm torque at **a** *W/D* = 2, **b** *W/D* = 3, **c** *W/D* = 4, and **d** *W/D* = 5

2.4.2 Regression analysis

Regression analysis [24] has been performed after fixing the geometry configuration of *E/D*, and *W/D* to be 4 as the joint with *E/D* and *W/D* $\geq$ 4 had the bearing failure mode. Regression analysis is performed to determine the influence of nanoclay and bolt pretension on the failure load of the composite joint. Regression investigates and models the relationship between a response, i.e., the failure load (*L*), and the predictors, i.e., the material type (*M*) and the torque (*T*) in the present study. In particular, regression analysis is often used to determine how the response variable changes with change in a particular predictor variable. The analysis of variance given in Table 14 shows the amount of variation in the response data explained by the predictors and the amount of variation left unexplained.

As shown in Table 14 (*P* value $< \alpha$ at 95% confidence interval), there is a valuable impact of the bolt pretension as well as the material variation on the failure load of the joint. The *P* value for regression is 0.000, indicating that at least one of the regression coefficients is significantly different than zero. From the *P* value and percentage contribution of the predictors, i.e., material and torque, as shown in Table 14, it is clearly visible that the response, i.e., failure load is largely influenced by the torque (*P* = 0.000) as compared to the material variation (*P* = 0.002). The predictive failure load values were determined using Eq. (8) which was given by regression:

$$L = 4739.8 + 197.2M + 363.2T, \quad (8)$$

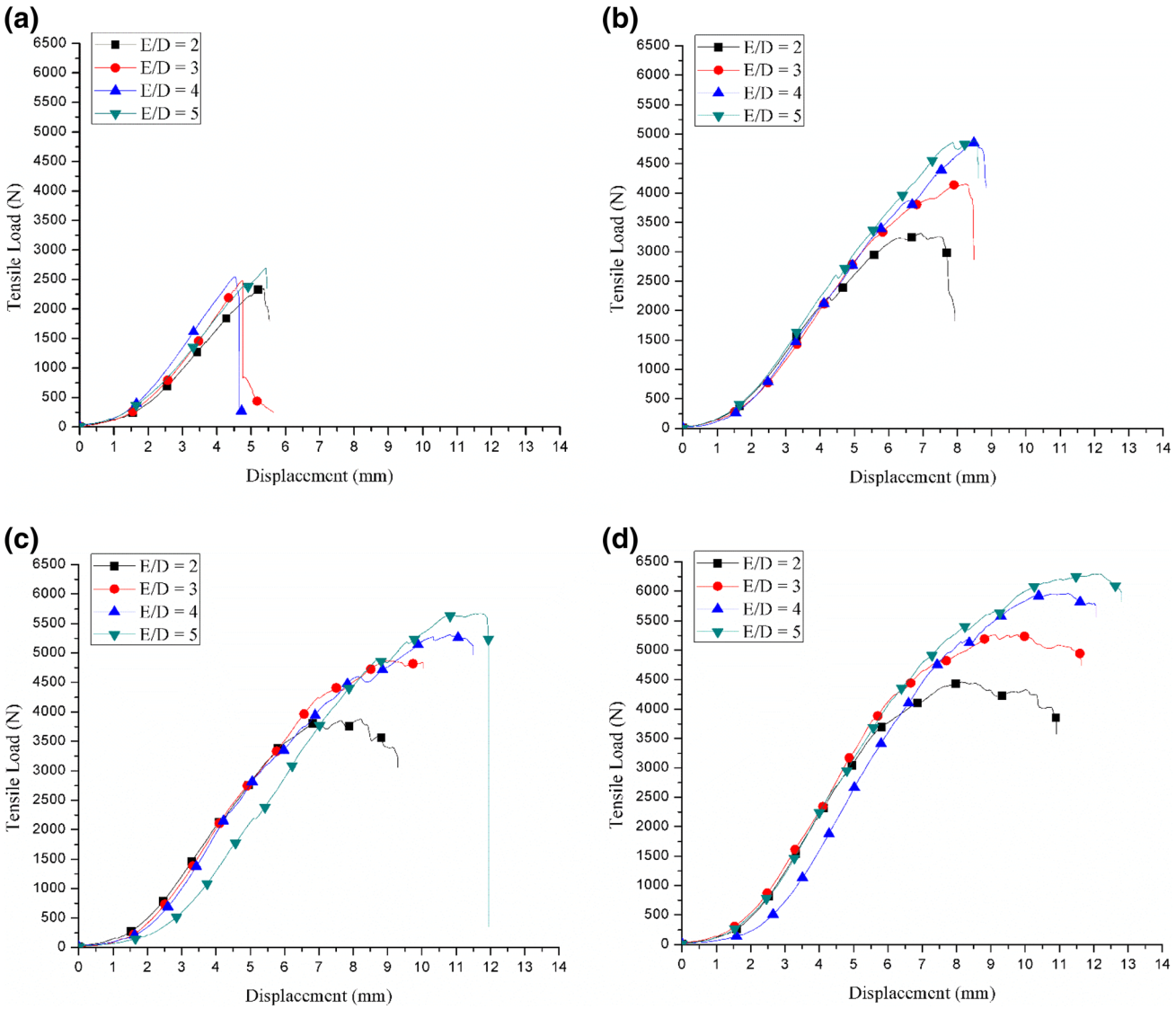

Fig. 10 Load vs displacement plots for the joints with nanoclay with 0 Nm torque at **a** *W*/*D* = 2, **b** *W*/*D* = 3, **c** *W*/*D* = 4, and **d** *W*/*D* = 5

where L is the failure load (in N), M is the material variation (wt% of nanoclay), and T is the torque (in Nm). The residual plot for the failure load is shown in Fig. 15. The percentage error in the experimental and the predicted value through the regression equation is less than 2.4%.

3 Numerical analysis

Finite element analysis of the single-lap bolted joint was performed using ANSYS structural analysis module. Material properties of the composite specimen were taken as given in Table 10. For the failure analysis of the joint progressive damage analysis along with the characteristic curve method has been performed.

3.1 Characteristic curve method

Stresses around the bolt hole in the composite plate are high due to stress concentration and evaluation of failure near the bolt hole may give premature results, which actually does not happen in real-life situations. Therefore, to overcome the problem of stress concentration, characteristic curve method has been used to predict the failure of the single-lap composite joint [5, 25]. The curve is drawn, as shown in Fig. 16 as per Eq. (9) using the characteristic lengths:

$$r_c = \frac{D}{2} + R_{ot} + (R_{oc} - R_{ot})\cos\theta, \tag{9}$$

where r_c is the radius of characteristic curve, D is diameter of the hole, R_{ot} is characteristic length in tension, and R_{oc} is characteristic length in compression. Angle, θ, can be

Table 13 Failure modes observed for different joint configurations

Set no.	Ratios		Failure mode	
	W/D	*E/D*	Neat	Clay
1	2	2	NT	NT
2	2	3	NT	NT
3	2	4	NT	NT
4	2	5	NT	NT
5	3	2	NT	NT
6	3	3	NT	NT
7	3	4	NT	NT
8	3	5	NT	NT
9	4	2	NT	NT
10	4	3	NT	B + NT
11	4	4	B + NT	B
12	4	5	B + NT	B
13	5	2	B	B
14	5	3	B	B
15	5	4	B	B
16	5	5	B	B

measured either clockwise or anticlockwise from the axis of applied load due to the symmetry of the curve.

In the present work, the characteristic lengths in tension and compression are obtained numerically. The finite element analysis has been performed on the open-hole laminates to determine the characteristic lengths in tension and compression [5].

The laminate was modeled with a particular *E/D* and *W/D* ratio. The laminate was subjected to the symmetrical tensile load (*F*). The mean tensile strength was calculated using Eq. (10):

$$\text{Mean tensile strength} = \frac{F}{(W-D)t}, \tag{10}$$

where *W* is the width of the plate, *D* is the diameter of the hole, and *t* is the thickness of the laminate. The point from the edge of the hole in the transverse direction was located, such that the equivalent stress is equal to the mean tensile strength. The distance from the hole edge to the point where the equivalent stress is equal to the mean tensile strength is called the characteristic length in tension.

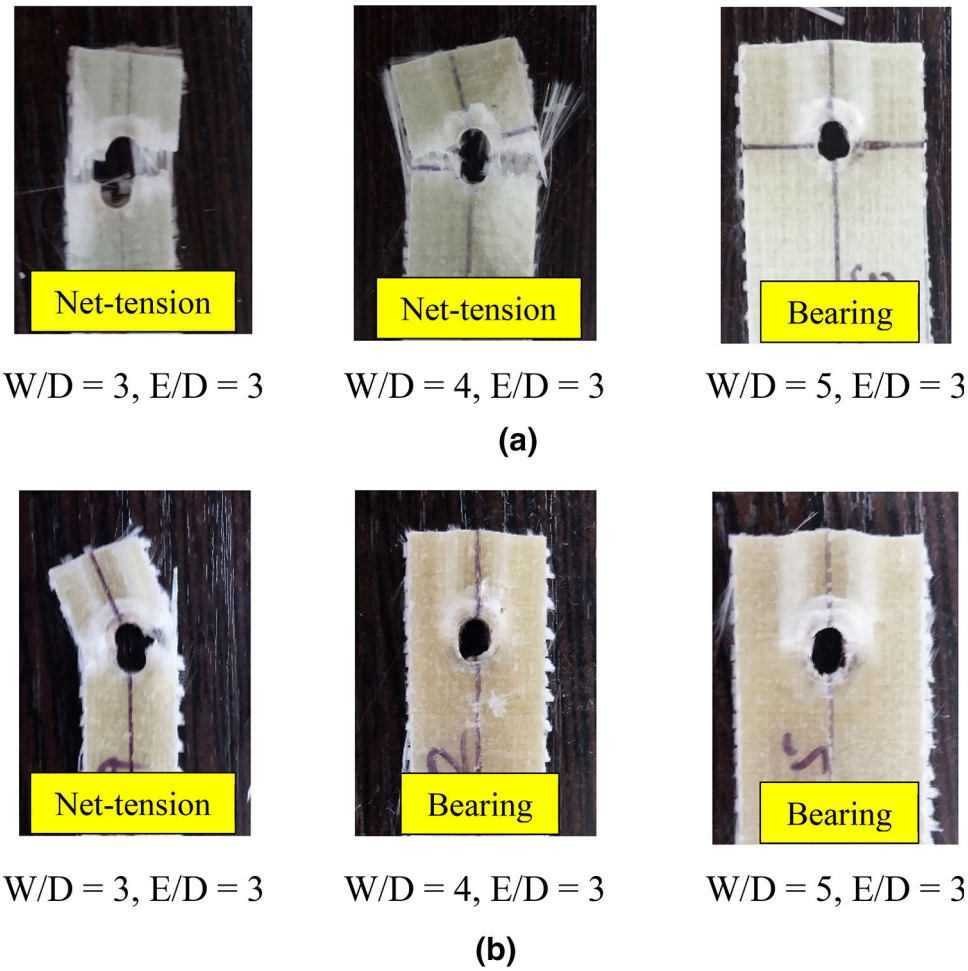

Fig. 11 Actual images of the specimens depicting the failure modes of the joints made of composite using **a** neat epoxy, and **b** epoxy modified with nanoclay

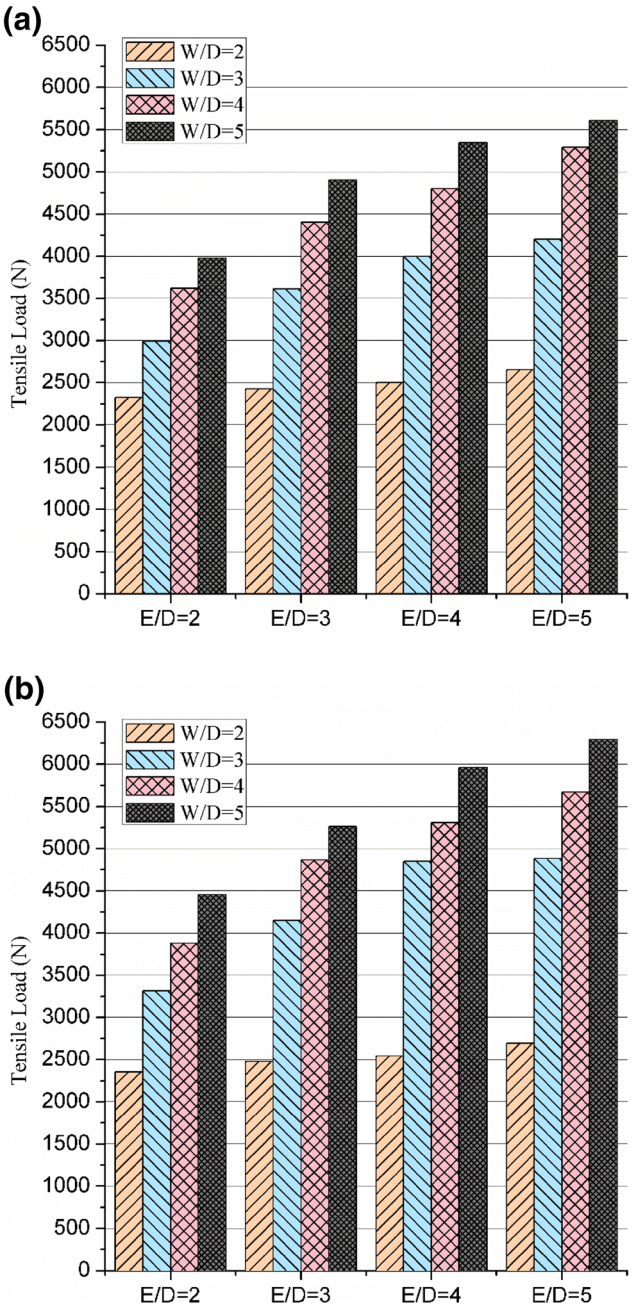

Fig. 12 Maximum failure loads for the joints with different *E/D* and *W/D* ratios made of composite using **a** neat epoxy, and **b** epoxy modified with nanoclay

A compressive force (F) was applied to the hole. The bearing strength of the specimen was calculated using Eq. (11):

$$\text{Mean bearing strength} = \frac{F}{Dt}, \tag{11}$$

where D is the diameter of the hole and t is the thickness of the laminate. Then, the point ahead of the hole was located, such that the equivalent stress was equal to the mean

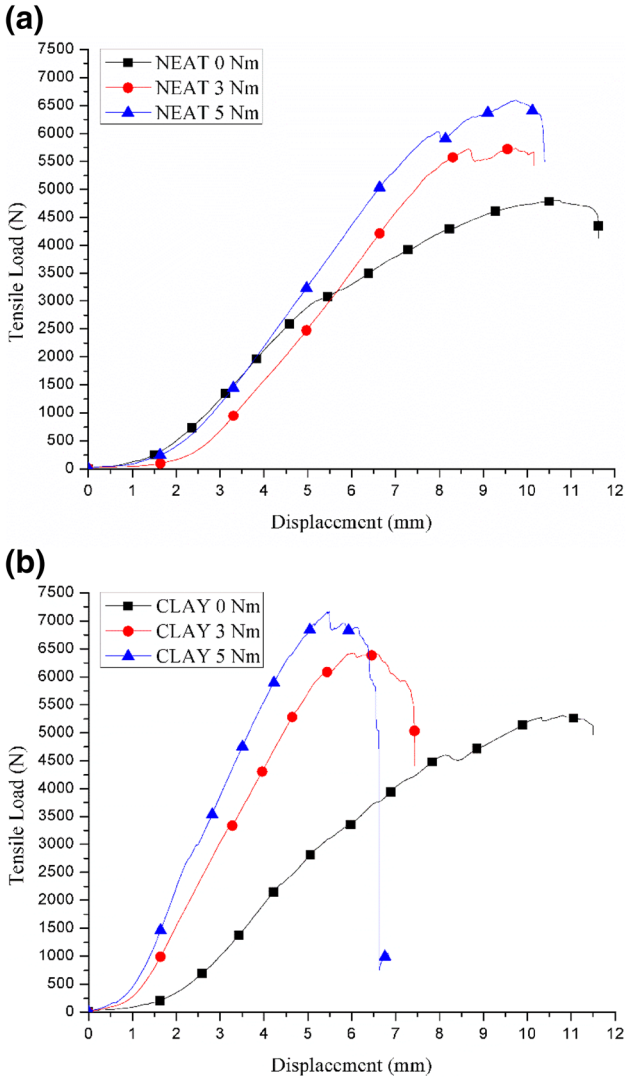

Fig. 13 Effect of torque on the failure load of the joint with $E/D = 4$ and $W/D = 4$ with **a** neat epoxy, and **b** epoxy modified with nanoclay

bearing strength. The distance from the edge of the hole to this point where the equivalent stress becomes equal to the mean bearing stress is called the characteristic length in compression.

For the damage initiation, Hashin failure criteria using Eqs. (12)–(15) were used to perform the progressive failure analysis of the composites.

Fiber failure used for tensile and compressive loadings in the longitudinal direction (fiber direction) is given in Eqs. (12) and (13), respectively:

$$f_f = \left(\frac{\sigma_1}{X_t}\right)^2 + \left(\frac{\tau_{12}}{S}\right)^2, \quad \sigma_1 \geq 0 \tag{12}$$

$$f_f = -\frac{\sigma_1}{X_c}, \quad \sigma_1 < 0. \tag{13}$$

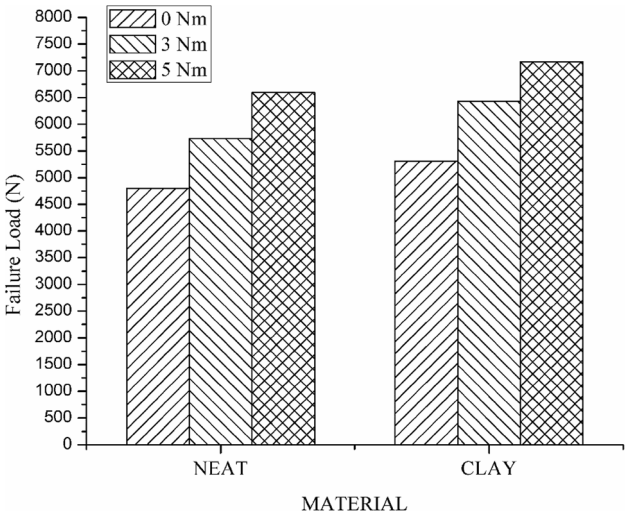

Fig. 14 Maximum failure loads for the joints with $E/D = 4$ and $W/D = 4$ at different torque settings

Matrix failure for tensile and compressive loadings in transverse direction is given by Eqs. (14) and (15), respectively:

$$f_{\mathrm{m}} = \left(\frac{\sigma_2}{Y_{\mathrm{t}}}\right)^2 + \left(\frac{\tau_{12}}{S}\right)^2, \quad \sigma_2 \geq 0 \tag{14}$$

$$f_{\mathrm{m}} = \left(\frac{\sigma_2}{2S}\right)^2 + \left(\frac{\tau_{12}}{S}\right)^2 + \left[\left(\frac{Y_{\mathrm{c}}}{2S}\right)^2 - 1\right]\frac{\sigma_2}{Y_{\mathrm{c}}}, \quad \sigma_2 < 0, \tag{15}$$

where f_{f} and f_{m} are the failure index for the fiber and the matrix. σ_1 and σ_2 are stresses setup in longitudinal and transverse directions, respectively, X_{t} and Y_{t} are tensile stress limits in longitudinal and transverse directions, S is shear stress in plane, and X_{c} and Y_{c} are compressive stress limits in longitudinal and transverse directions. In Hashin's equations, $X_{\mathrm{t}} = Y_{\mathrm{t}}$ and $X_{\mathrm{c}} = Y_{\mathrm{c}}$ because of the woven fabric used in the present work. Maximum failure index ($\mathrm{FI}_{\max}$), the maximum value among f_{f} and f_{m} in tension and compression, is used for determining the failure modes and the failure loads. Based on the location of maximum failure index on the characteristic curve, failure modes have been identified. Equation (16) gives the failure modes on the basis of angle (θ_{f}) measured on the characteristic curve:

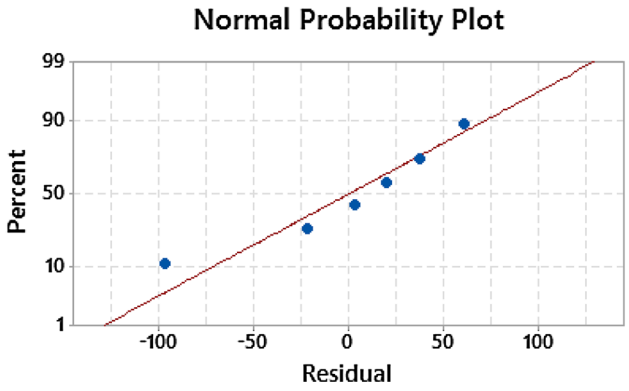

Fig. 15 Residual plots for the failure load

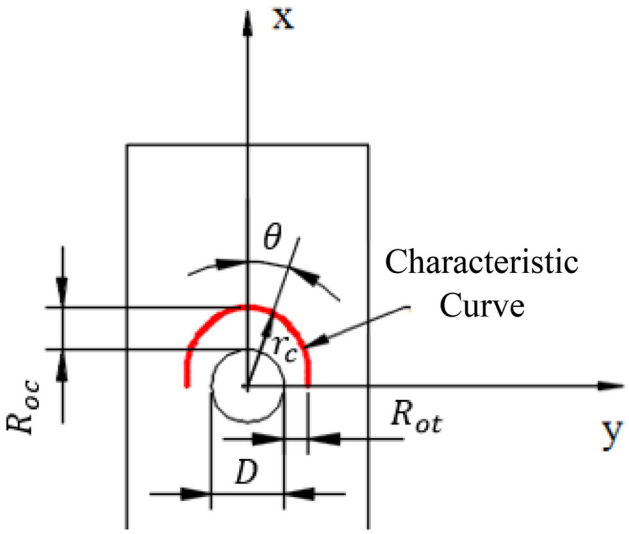

Fig. 16 Description of the characteristic curve

$$\begin{aligned} &0^\circ \leq \theta_{\mathrm{f}} \leq 15^\circ : \text{Bearing}, \\ &30^\circ \leq \theta_{\mathrm{f}} \leq 60^\circ : \text{Shear-out}, \\ &75^\circ \leq \theta_{\mathrm{f}} \leq 90^\circ : \text{Net-tension}. \end{aligned} \tag{16}$$

Failure load of the single-lap composite joint is determined using Eq. (17):

$$\text{Failure load} = \frac{F}{\mathrm{FI}_{\max}}, \tag{17}$$

Table 14 Analysis of variance for failure loads

Source	*df*	Adj SS	Adj MS	*F* value	*P* value	Percentage contribution
Regression	2	3,867,125	1,933,563	376.92	0.000	–
M	1	525,104	525,104	102.36	0.002	13.52
T	1	3,342,021	3,342,021	651.49	0.000	86.08
Error	3	15,390	5130			0.39
Total	5	3,882,515				

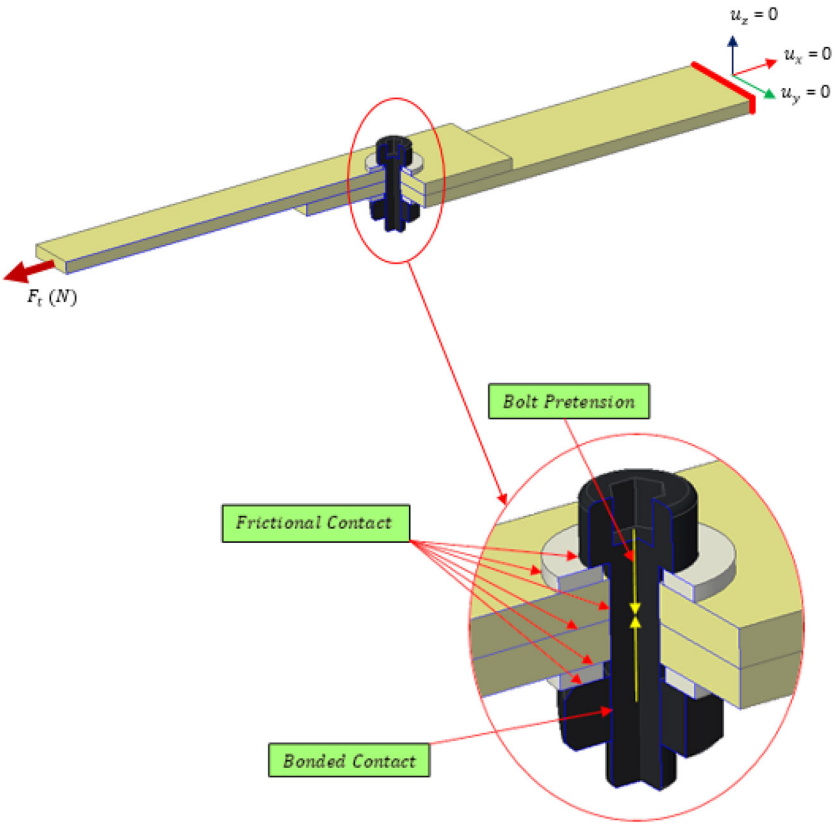

Fig. 17 Loads, boundary conditions, and contacts' setup in the numerical analysis of the joint

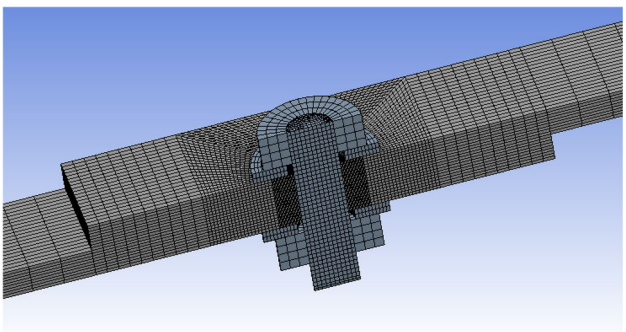

Fig. 18 Complete mesh of the single-lap joint

where F and FI_{max} are the values of applied force and maximum value of failure index, respectively.

3.2 Loads and boundary conditions

The applied loads, boundary conditions, and contact regions for the finite-element analysis are shown in Fig. 17. One side of the lap joint is fixed in all the directions, while, on the other side of the joint, an arbitrary tensile load, F_t of 4000 N is applied. Frictional contact behavior has been considered in all contact regions except the contact

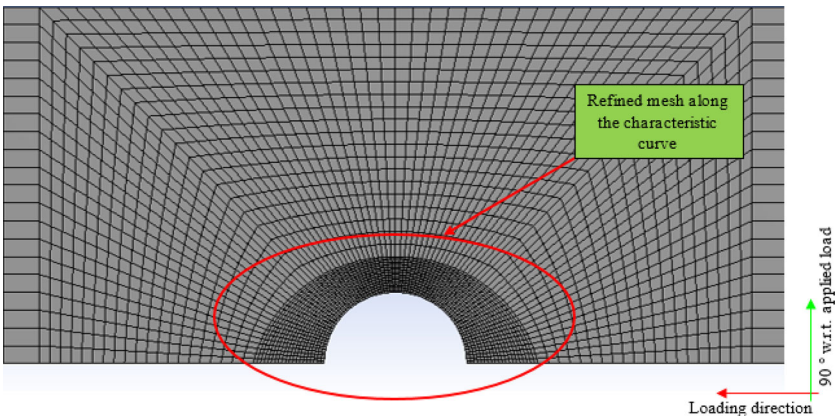

Fig. 19 Refined mesh around the hole in the composite joint

Table 15 Failure loads obtained from numerical analysis of the joint for different levels of geometric parameters

Set no.	Geometry level		Failure load (N)	
	W/D	*E/D*	Neat	Clay
1	2	2	2510	2602
2	2	3	2532	2624
3	2	4	2537	2630
4	2	5	2539	2658
5	3	2	3140	3411
6	3	3	3771	4350
7	3	4	4168	5036
8	3	5	4415	4884
9	4	2	3785	4076
10	4	3	4598	5116
11	4	4	5045	5590
12	4	5	5512	5945
13	5	2	4152	4644
14	5	3	5056	5542
15	5	4	5639	6279
16	5	5	5817	6546

between nut and bolt which represents the locked condition and is taken as bonded. Complete mesh of single-lap joint is shown in Fig. 18. Multizone mesh method has been used with all quad elements. Mesh density was determined by performing the convergence study. A refined mesh used along the characteristic curve is shown in Fig. 19. Analysis has been done in two steps. In the first step, bolt pretension is applied; and in the second step, bolt pretension is locked and tensile load is applied.

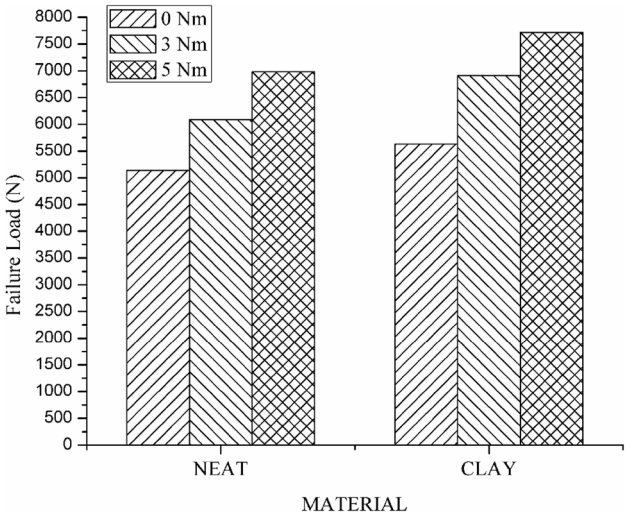

Fig. 21 Maximum failure loads for the joints with *E/D* = 4 and *W/D* = 4 at different torque settings

The failure loads predicted by the numerical analysis of the single-lap composite joint are shown in Table 15. It can be seen from the table that the numerical results fairly match with the experimental results.

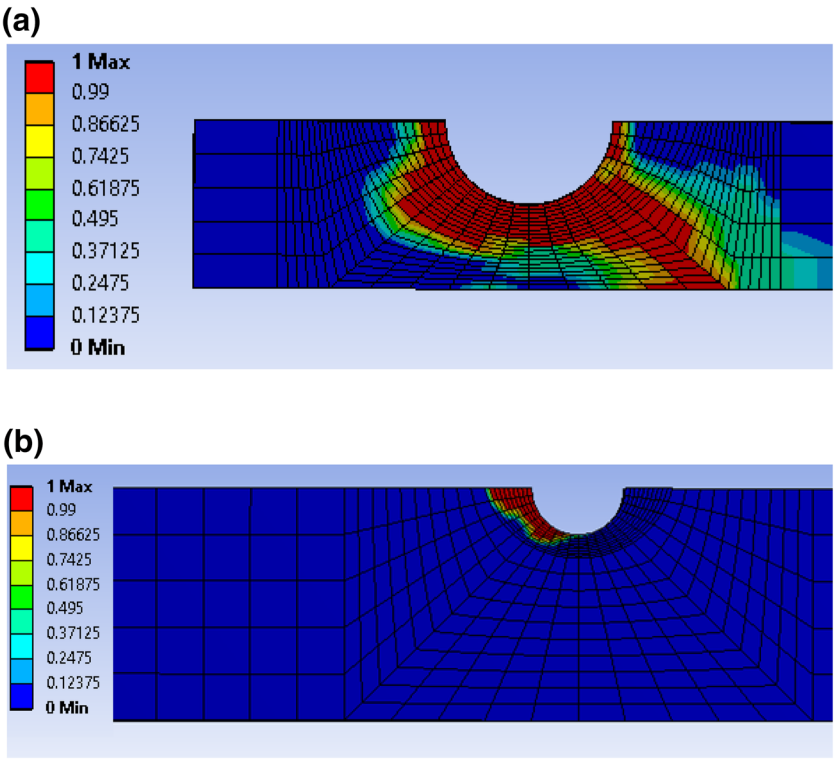

Fig. 20 Damage status of the composite joint for **a** *W/D* = 2 and *E/D* = 2, **b** *W/D* = 5 and *E/D* = 5

The damage status for the lowest and highest joint configurations is shown in Fig. 20. It can be seen from the figure that for the low width specimen, i.e., $W/D = 2$ the damage begins near the hole and progress towards the side edge leading to the net-tension failure mode. Therefore, it is again confirmed through the numerical analysis that the specimens with a low value of W/D fail in a sudden manner and is catastrophic in nature which should be avoided. It is due to the less material margin available to the sides of the hole. Whereas, for the high width specimen, i.e., $W/D = 5$, the damage begins around the hole and progress towards the free edge but could not reach the free end and represents the bearing failure mode.

Damage to the inner and outer layers is different due to the eccentricity of the applied load. Layers near the washer are under compression, whereas layers near the neutral axis, i.e., mating contact of the two composite plates are under tension due to out of plane displacement. Therefore, maximum damage in any of the layer through the thickness of the composite plate has been considered for the failure analysis.

The maximum numerically predicted failure load for the single-lap joint with $E/D = 4$ and $W/D = 4$ is shown in Fig. 21. It is clearly visible that the failure load increases with increase in the bolt pretension.

4 Conclusions

In the present work, the effect of molding parameters, nanoclay, and bolt preloads on the failure of single-bolt lap joints prepared from glass fiber reinforced nanocomposite laminates has been investigated. Based on the experimental and numerical results, the following conclusions have been drawn:

- Increasing the nanoclay concentration from 0 to 3 wt% has increased the strength of the composite laminate. Further increase in nanoclay wt% diminished the strength of the material. Incorporating 3 wt% of nanoclay, an improvement of 20, 21, and 10% was observed in tensile, compressive, and shear strength of the composite laminates, respectively. The optimum strength was achieved with a pressure of 140 kN, temperature of 150 °C, and holding time of 30 min in the compression molding.
- Failure load of the bolt joint increases by increasing E/D and W/D ratios. However, for the low value of $W/D = 2$, there is no effect of E/D ratio on the joint failure load.
- Net-tension failure mode has been observed for $W/D = 2$–3. Bolt joints with $W/D = 5$ failed in the pure bearing. For $W/D = 4$, the initial failure mode was bearing followed by secondary bending leading to net-tension failure.
- Incorporating 3 wt% of nanoclay has shown improvement in failure load of the bolt joints. A maximum of 21% improvement has been reported for $W/D = 3$ and $E/D = 3$ joint configuration.
- Increasing bolt preload has shown an increase in the failure load and stiffness of the bolt joint. For joints without nanoclay, failure load has been improved by 19 and 37% having preloads of 3 and 5 Nm, respectively. Similarly, 21 and 35% improvement is observed for joints prepared with nanoclay having preloads of 3 and 5 Nm, respectively.
- Numerical analysis has been performed for all design configurations using characteristic curve method and Hashin failure criteria. A good agreement is observed between numerical and experimental results.

References

1. Sen F, Pakdil M, Sayman O, Benli S (2008) Experimental failure analysis of mechanically fastened joints with clearance in composite laminates under preload. Mater Des 29(6):1159–1169
2. McCarthy MA, McCarthy CT, Lawlor VP, Stanley WF (2005) Three-dimensional finite element analysis of single-bolt, single-lap composite bolted joints: part I—model development and validation. Compos Struct 71(2):140–158
3. Zhai Y, Li D, Li X, Wang L, Yin Y (2015) An experimental study on the effect of bolt-hole clearance and bolt torque on single-lap, countersunk composite joints. Compos Struct 127:411–419
4. Qin T, Zhao L, Zhang J (2013) Fastener effects on mechanical behaviors of double-lap composite joints. Compos Struct 100:413–423
5. Zhang J, Liu F, Zhao L, Chen Y, Fei B (2014) A progressive damage analysis based characteristic length method for multi-bolt composite joints. Compos Struct 108:915–923
6. Atas A, Soutis C (2014) Strength prediction of bolted joints in CFRP composite laminates using cohesive zone elements. Compos B Eng 58:25–34
7. Egan B, McCarthy CT, McCarthy MA, Frizzell RM (2012) Stress analysis of single-bolt, single-lap, countersunk composite joints with variable bolt-hole clearance. Compos Struct 94(3):1038–1051
8. Gray PJ, O'Higgins RM, McCarthy CT (2014) Effects of laminate thickness, tapering and missing fasteners on the mechanical behaviour of single-lap, multi-bolt, countersunk composite joints. Compos Struct 107:219–230
9. Arun KV, Kumar DS, Murugesh MC (2014) Influence of bolt configuration and TiO_2/ZnS fillers content on the strength of composites fasteners. Mater Des 53:51–57
10. Sekhon M, Saini JS, Singla G, Bhunia H (2017) Influence of nanoparticle fillers content on the bearing strength behavior of glass fiber-reinforced epoxy composites pin joints. Proc Inst Mech Eng Part L J Mater Des Appl 231(8):641–656
11. Asi O (2010) An experimental study on the bearing strength behavior of Al_2O_3 particle filled glass fiber reinforced epoxy composites pinned joints. Compos Struct 92(2):354–363

12. Liu L, Zhang B-M, Wang D-F, Wu Z-J (2006) Effects of cure cycles on void content and mechanical properties of composite laminates. Compos Struct 73(3):303–309
13. Singh M, Saini JS, Bhunia H, Singh P (2017) Application of Taguchi method in the optimization of geometric parameters for double pin joint configurations made from glass–epoxy nanoclay laminates. J Compos Mater 51(19):2689–2706
14. Pandey RK, Panda SS (2015) Multi-performance optimization of bone drilling using Taguchi method based on membership function. Measurement 59:9–13
15. Ghani JA, Choudhury IA, Hassan HH (2004) Application of Taguchi method in the optimization of end milling parameters. J Mater Process Technol 145(1):84–92
16. Nalbant M, Gökkaya H, Sur G (2007) Application of Taguchi method in the optimization of cutting parameters for surface roughness in turning. Mater Des 28(4):1379–1385
17. Ghaffari M, Ehsani M, Khonakdar HA, Van Assche G, Terryn H (2012) The kinetic analysis of isothermal curing reaction of an epoxy resin-glassflake nanocomposite. Thermochim Acta 549:81–86
18. Ghaemy M, Riahy MH (1996) Kinetics of anhydride and polyamide curing of bisphenol A-based diglycidyl ether using DSC. Eur Polym J 32(10):1207–1212
19. Timmerman JF, Hayes BS, Seferis JC (2002) Nanoclay reinforcement effects on the cryogenic microcracking of carbon fiber/epoxy composites. Compos Sci Technol 62(9):1249–1258
20. Haque A, Shamsuzzoha M, Hussain F, Dean D (2003) S2-glass/epoxy polymer nanocomposites: manufacturing, structures, thermal and mechanical properties. J Compos Mater 37(20):1821–1837
21. Kornmann X, Rees M, Thomann Y, Necola A, Barbezat M, Thomann R (2005) Epoxy-layered silicate nanocomposites as matrix in glass fibre-reinforced composites. Compos Sci Technol 65(14):2259–2268
22. Chowdhury FH, Hosur MV, Jeelani S (2006) Studies on the flexural and thermomechanical properties of woven carbon/nanoclay-epoxy laminates. Mater Sci Eng A 421(1):298–306
23. Novak BM (1993) Hybrid nanocomposite materials—between inorganic glasses and organic polymers. Adv Mater 5(6):422–433
24. Armagan M, Arici AA (2017) Cutting performance of glass–vinyl ester composite by abrasive water jet. Mater Manuf Processes 32(15):1715–1722
25. Chang FK, Scott RA, Springer GS (1982) Strength of mechanically fastened composite joints. J Compos Mater 16(6):470–494